Toward Understanding the Mechanism of the Complex Cyclization Reaction Catalyzed by Imidazole Glycerolphosphate Synthase: Crystal Structures of a Ternary Complex and the Free Enzyme[†,‡]

Barnali N. Chaudhuri,[#,||] Stephanie C. Lange,[#,⊥] Rebecca S. Myers,[§] V. Jo Davisson,[§] and Janet L. Smith*[,#]

Departments of Biological Sciences and Medicinal Chemistry & Molecular Pharmacology, Purdue University, West Lafayette, Indiana 47907 USA

Received February 25, 2003; Revised Manuscript Received April 1, 2003

ABSTRACT: Imidazole glycerol phosphate synthase catalyzes formation of the imidazole ring in histidine biosynthesis. The enzyme is also a glutamine amidotransferase, which produces ammonia in a glutaminase active site and channels it through a 30-Å internal tunnel to a cyclase active site. Glutaminase activity is impaired in the resting enzyme, and stimulated by substrate binding in the cyclase active site. The signaling mechanism was investigated in the crystal structure of a ternary complex in which the glutaminase active site was inactivated by a glutamine analogue and the unstable cyclase substrate was cryo-trapped in the active site. The orientation of N^1-(5′-phosphoribulosyl)-formimino-5-aminoimidazole-4-carboxamide ribonucleotide in the cyclase active site implicates one side of the cyclase domain in signaling to the glutaminase domain. This side of the cyclase domain contains the interdomain hinge. Two interdomain hydrogen bonds, which do not exist in more open forms of the enzyme, are proposed as molecular signals. One hydrogen bond connects the cyclase domain to the substrate analogue in the glutaminase active site. The second hydrogen bond connects to a peptide that forms an oxyanion hole for stabilization of transient negative charge during glutamine hydrolysis. Peptide rearrangement induced by a fully closed domain interface is proposed to activate the glutaminase by unblocking the oxyanion hole. This interpretation is consistent with biochemical results [Myers, R. S., et al., (2003) *Biochemistry 42*, 7013−7022, the accompanying paper in this issue] and with structures of the free enzyme and a binary complex with a second glutamine analogue.

Imidazole glycerol phosphate synthase (IGPS)[1] catalyzes the fifth step of the nine-step histidine biosynthetic pathway in microbes, fungi, and plants, forming the imidazole ring of the histidine precursor imidazole glycerol phosphate (ImGP; (*1*−*3*)). IGPS converts N^1-(5′-phosphoribulosyl)-formimino-5-aminoimidazole-4-carboxamide ribonucleotide (PRFAR) to ImGP and 5′-(5-aminoimidazole-4-carboxamide) ribonucleotide (AICAR) (Figure 1a). AICAR is also an entry point to the purine biosynthetic pathway.

IGPS catalyzes two tightly coupled reactions in distinct active sites (*1*).

$$\text{glutamine} + H_2O \rightarrow \text{glutamic acid} + NH_3$$

$$\text{PRFAR} + NH_3 \rightarrow \text{ImGP} + \text{AICAR}$$

In plants and fungi, the two catalytic domains are fused, while in bacteria the catalytic functions are performed by separate polypeptides of a heterodimeric protein (HisH for the glutaminase reaction and HisF for the cyclase reaction). The overall domain organization was demonstrated in the crystal structure of intact IGPS from yeast (His7) inactivated by a covalently bound glutamine analogue (*4*). An N-terminal glutamine amidotransferase domain (*5*) generates the ammonia nucleophile, which is channeled to the PRFAR active site. IGPS belongs to the triad family of amidotransferases, having a conserved Cys−His−Glu catalytic triad in the glutaminase active site (*6*). The C-terminal cyclase domain is a $(\beta/\alpha)_8$ barrel domain, housing the PRFAR active site at the top of the barrel (*4*, *7*). Sequence and structural similarity within the cyclase domain is suggestive of an ancient gene duplication of half barrels to form the whole barrel (*7*, *8*).

The overall reaction catalyzed by the cyclase domain of IGPS is intriguing from a mechanistic point of view (*9*). ImGP synthesis involves steps of NH_3-dependent C−N ligase, C−N lyase, and C−N cycloligase, the order and

[†] This work was supported by NIH Grants DK42303 and GM24268 to J.L.S. and GM45756 to V.J.D.

[‡] Structures are available in the Protein Data Bank with accession codes 1OX5 for the ternary complex, 1OX4 for the DON-inactivated enzyme, and 1OX6 for the apo-enzyme.

* To whom correspondence should be addressed: Department of Biological Sciences, Purdue University, 915 W. State St., West Lafayette, IN 47907-2054. E-mail: smithj@purdue.edu. Phone: (765) 494−9246. FAX: (765) 496−1189.

[#] Department of Biological Sciences.

[§] Department of Medicinal Chemistry & Molecular Pharmacology.

[||] Present address: UCLA-DOE Center for Genomics and Proteomics, University of California, Los Angeles, CA 90095 USA.

[⊥] Present address: Dept. of Biochemistry and Molecular Biology, Indiana University School of Medicine, Indianapolis, IN 46202 USA.

[1] Abbreviations: AICAR, 5′-(5-aminoimidazole-4-carboxamide) ribonucleotide; DON, 6-diazo-5-oxo-L-norleucine; IGPS, imidazole glycerol phosphate synthase; ImGP, imidazole glycerol phosphate; PRFAR, N^1-(5′-phosphoribulosyl)-formimino-5-aminoimidazole-4-carboxamide ribonucleotide; RMSD, root-mean-square deviation.

10.1021/bi034320h CCC: $25.00
Published on Web 05/23/2003

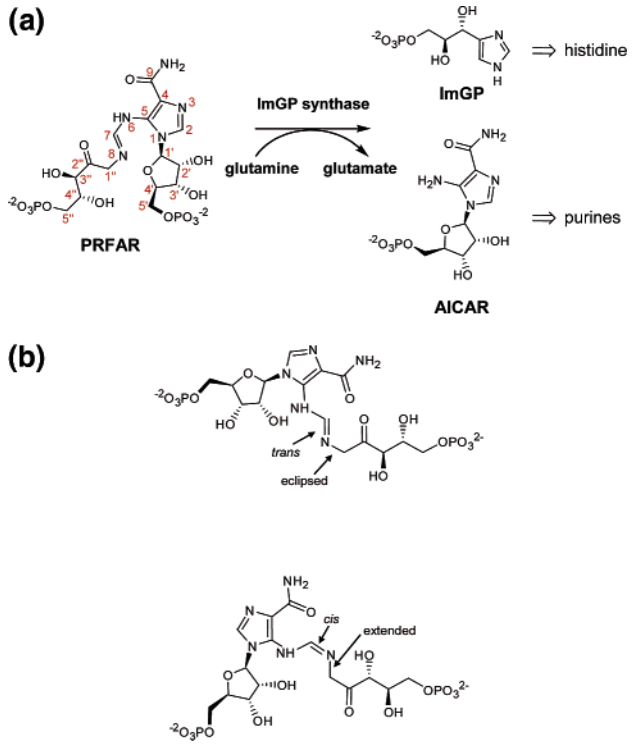

FIGURE 1: IGPS reaction chemistry. (a) Overall chemical reaction of IGPS. Atom numbering for the substrate PRFAR is shown in this schematic diagram. (b) The "*trans*-eclipsed" and "*cis*-extended" conformers of PRFAR. Both are compatible with the PRFAR electron density. With the exception of the labeled bonds, the drawings are schematic and do not represent actual conformations.

mechanism of which are not fully established (*1*, *10*, *11*). A knowledge of the binding of substrate PRFAR to the cyclase active site is essential to understanding the reaction mechanism, and also would assist inhibitor design. Binding sites for the phosphate end groups of PRFAR were inferred from the positions of phosphate or sulfate ions in crystal structures of IGPS from yeast and bacteria (*4*, *7*, *12*, *13*). However, these structures do not show how IGPS binds the central atoms of PRFAR, where catalysis occurs. Biochemical studies together with site-directed mutagenesis shed light on potentially important residues at the PRFAR active site (*11*, *14*).

Substrate tunneling and cross-talk between remote active sites are two interesting and familiar aspects of the function of glutamine amidotransferases (*5*, *15*). These events are now established with extensive structural and biochemical work on PRPP amidotransferase (*16*−*18*) and on carbamoyl phosphate synthetase (*19*−*22*). In IGPS, a new and distinct organization of active sites has evolved to ensure efficient NH_3 transfer. The glutaminase active site of IGPS generates NH_3 at the domain interface, close to the bottom of the cyclase $(\beta/\alpha)_8$ barrel. A discontinuous tunnel through the barrel joins the domain interface at the bottom to the PRFAR active site at the top. The hydrophobic barrel interior is thus a functional NH_3 tunnel, which is a novel use of a $(\beta/\alpha)_8$ barrel. A "gate" of four charged residues at the bottom of the barrel appears to control the entry of NH_3 to the hydrophobic tunnel. The hydrophobic tunnel and charge gate are common features in the structures of intact yeast (*4*) and bacterial (*13*, *23*) IGPS and of two bacterial HisF subunits (*7*, *12*).

Catalysis in the two active sites is tightly coupled, such that glutaminase activity is negligible in absence of the cyclase substrate PRFAR. The binding of PRFAR at the top of the barrel signals the glutaminase domain, and results in a 4900-fold increase in k_{cat}/K_m for glutaminase (*14*). An unformed oxyanion hole was postulated as the basis for low glutaminase activity in the PRFAR-free form of the yeast enzyme (*4*). Structures of intact IGPS from yeast and bacteria (*4*, *13*, *23*) and of bacterial HisH (*13*, *24*) reveal somewhat different conformations for the presumed oxyanion binding site. Sequence conservation together with surface complementarity at the domain interface led us to propose a central role for the docking surfaces in mediating cross-talk between the cyclase and glutaminase active sites, which are 30 Å apart (*4*). However, only a few details have been worked out concerning the mechanism of signaling upon PRFAR binding.

Here we describe structures of (i) a complex of the substrate PRFAR and IGPS covalently modified by the glutamine analogue acvicin at 2.5 Å, (ii) apo IGPS at 2.4 Å, and (iii) IGPS inactivated by the glutamine analogue 6-diazo-5-oxo-L-norleucine (DON) at 2.5 Å. The PRFAR complex describes the PRFAR active site in detail, providing further insight into the enzymatic reaction mechanism. Comparison of the free, acivicin-, and DON-inactivated forms of the glutaminase active site reveals structural changes relevant to activation. The PRFAR-bound and -free forms of IGPS shed light on flexible parts of the molecule with potential roles in crosstalk between active sites.

MATERIALS AND METHODS

Crystallization. Crystals of a PRFAR complex of IGPS ("IGPS−PRFAR") were grown as described previously (*4*). This included preincubation with acivicin and PRFAR. Acivicin inactivated the protein at Cys83. PRFAR, which is unstable, did not survive crystallization. A crystal was washed in the crystallization reservoir solution (0.2 M $(NH_4)_2SO_4$ in solution A (22−28% PEG MME 5000, 0.1 M MES pH 6.5−7.0)), and soaked 15 min in solution A. The crystal was then soaked 45 min in solution A plus 10 mM PRFAR. The crystal was cryoprotected by a quick dunk in the latter solution plus 25% ethylene glycol, and flash-frozen in a cold N_2 stream. Crystals of the free enzyme ("apo-IGPS") were grown as described previously, excluding preincubation with PRFAR and acivicin. Crystals of DON-inactivated IGPS ("IGPS−DON") were grown as described previously, except that the protein was preincubated in a solution containing protein, PRFAR and DON in a 1:1:5 molar ratio.

Data Collection and Refinement. All data were recorded at ID19 at the Advanced Photon Source, and processed and scaled with the HKL2000 package (*25*) (Table 1). Crystals for all structures reported here were roughly isomorphous with those for the 2.1-Å structure of IPGS inactivated by acivicin (*4*), which was the starting point for refinement after deletion of nonprotein atoms. Like the original acivicin complex, apo IGPS and the IGPS−PRFAR and IGPS-DON complexes crystallized in orthorhombic space group $P2_12_12_1$ with two molecules in the asymmetric unit. All starting models were subjected to rigid-body refinement of individual domains using data to 3-Å spacings. Atomic refinement was done using successive cycles of a high-temperature, simulated-

Table 1: Crystallographic Data[a]

	IGPS−PRFAR	apo IGPS	IGPS−DON
space group	$P2_12_12_1$	$P2_12_12_1$	$P2_12_12_1$
unit cell dimensions (Å)	98.8, 111.5, 117.2	97.0, 112.0, 114.8	98.5, 112.0, 115.3
data range (Å)	100−2.5 (2.59−2.5)	50−2.4 (2.49−2.4)	100−2.5 (2.59−2.5)
R-merge[b]	0.102 (0.52)	0.106 (0.46)	0.098 (0.33)
average multiplicity	8.9 (8.4)	4.2 (4.0)	6.5 (5.8)
average I/σ_I	23.6 (3.5)	11.6 (2.2)	16.7 (3.0)
unique reflections	45678	47205	45173
completeness (%)	100 (100)	92.9 (93.5)	99.8 (99.8)

[a] Numbers in parentheses correspond to the highest resolution shell. [b] $R_{merge} = \Sigma_h\Sigma_i|I_{h,i} - \langle I_h\rangle|/\Sigma_h\Sigma_i|I_{h,i}|$.

Table 2: Refinement Summary

	IGPS−PRFAR	apo IGPS	IGPS−DON
no. of reflections used ($F > 0$)	45460	46100	44777
d_{min} (Å)	2.5	2.4	2.5
no. of non-hydrogen atoms	8532	8575	8575
bound substrate/inhibitor	PRFAR, acivicin		DON
R_{factor}[a]	0.223	0.228	0.228
R_{free}[a]	0.246	0.255	0.260
RMSD bond length (Å)[b]	0.008	0.007	0.006
RMSD bond angle (°)[b]	1.37	1.35	1.26
average B (Å^2) all atoms[c]	33.2	37.8	37.7
average B (Å^2) protein[c]	32.5	37.7	37.6
average B ligand (Å^2)[c]	41.1		42.7
RMSD B-bonded (Å^2)[c]	1.5	1.6	1.5
estimated coordinate error (σ_A based) (Å)[b]	0.31	0.28	0.31

[a] $R_{factor} = \Sigma||F_{obs}| - |F_{calc}||/\Sigma|F_{obs}|$. $R_{free} = R_{factor}$ for a subset of reflections not included in the refinement. F_{obs} and F_{calc} are observed and calculated structure factors. [b] Calculated in CNS (*27*). [c] Calculated in MOLEMAN (*41*).

annealing protocol (*26*) in CNS (*27*) and manual rebuilding in O (*28*). Thermal motion was modeled as two temperature factors per residue until the final step of the refinement when individual isotropic temperature factors were refined; an overall anisotropic temperature factor was used throughout refinement. As observed in the previously reported structure (*4*), all three structures included a Ni^{2+} complex, and those lacking PRFAR had either sulfate of pyrophosphate ions in the cyclase active site. Noncrystallographic symmetry restraints were imposed separately on the glutaminase and cyclase domains, excluding the N-terminal four residues and coordinated Ni^{2+}. Less well-ordered regions of the proteins were modeled as closely as possible to the original high-resolution structure. As in the original structure, a few loops in each structure were disordered and not modeled. The IGPS−DON structure includes four residues in the α2−β2 loop of the cyclase domain that were missing in the original structure. Ligands were modeled in the $|F_o| - |F_c|$ difference density using substructures from the Cambridge Structure Database (*29*) or the PDB (*30*). The central five atoms of PRFAR apparently have multiple conformations, which are similar enough to produce continuous density. Several models for these atoms were tested in refinement in an effort to minimize phase bias. Ligand dictionaries were built using XPLO2D (*31*). Stereochemical checks performed using WHATIF (*32*) were satisfactory. The Ramachandran plot, computed using PROCHECK (*33*), includes three disallowed conformations supported by density and also observed in the original structure. Refinement statistics for the final models are in Table 2.

RESULTS

The IGPS complexes described here are similar in overall structure and domain orientation to the previously reported structure (*4*), Figure 2a. Cα atoms superimpose with RMSDs of 0.5 Å or less. Yeast IGPS is a monomer with a glutaminase domain similar to the bacterial HisH subunit and a cyclase domain similar to the bacterial HisF subunit. We refer to secondary structural elements by sequential numbering for each domain, with a prefix of "h" or "f" for the glutaminase and cyclase domains, respectively. Secondary structures in the $(\beta/\alpha)_8$ barrel cyclase domain are numbered according to the familiar barrel architecture (β1, α1, β2, α2, etc., β8, α8). Two additional helices at the top of the barrel are referred to as α4′ and α8′ because of their positions between β4 and α4, and β8 and α8, respectively.

PRFAR Complex and Cyclase Active Site. The structure of IGPS in complex with PRFAR provides the first view of substrate binding in the cyclase active site. PRFAR binds to a long, narrow cleft extending across the top of the cyclase $(\beta/\alpha)_8$ barrel domain, with the terminal phosphate groups at the N-termini of helical insertions α4′ and α8′ on opposite sides of the barrel. Each phosphate group forms four hydrogen bonds with protein groups, predominantly backbone NHs of conserved glycines, as well as a few water-bridged hydrogen bonds. These interactions are similar to those seen in the sulfate and phosphate complexes of the fungal and bacterial enzymes (*4*, *7*, *12*, *13*).

The end-to-end orientation of the extended PRFAR molecule was defined unambiguously by the electron density (Figure 3). The AICAR end of PRFAR binds to the α4′ side of the active site, and the glycerol phosphate end of PRFAR to the α8′ side. The binding orientation is relevant to catalysis, and also to the mechanism of interdomain signaling, which can be induced more strongly by the product ImGP than by the product AICAR (*14*). Electron density is very clear for the glycerol phosphate and the hydroxyl positions are well determined. The glycerol phosphate group interacts

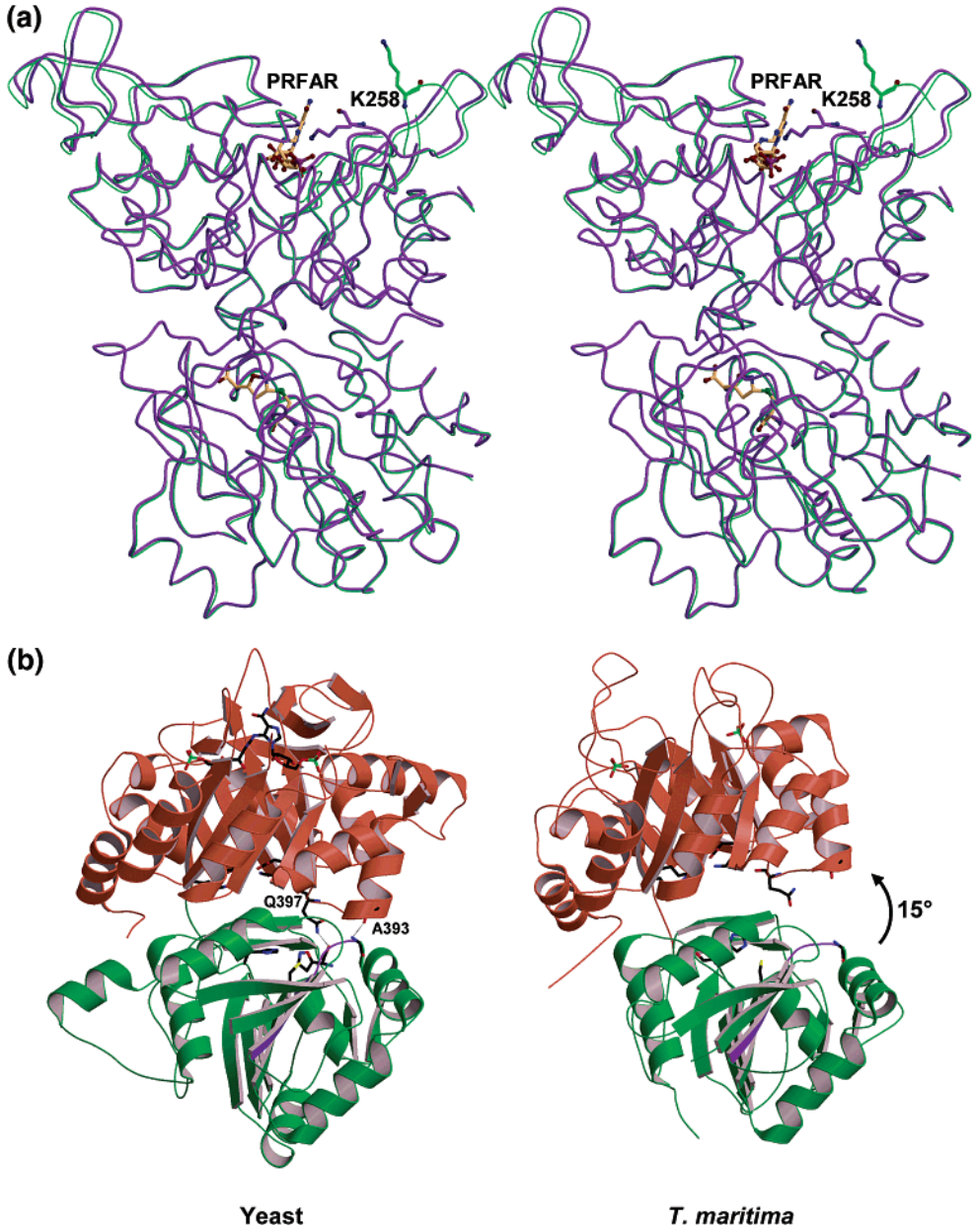

FIGURE 2: Overall fold of IGPS. (a) Comparison of yeast IGPS with and without PRFAR. The molecules are superimposed as line drawings of IGPS−PRFAR (magenta) and apo-IGPS (green) in this stereo diagram. The different positions for Lys258 are apparent; Lys258, PRFAR, and acivicin are drawn as ball-and-stick. (b) Comparison of yeast (left) and bacterial IGPS (right). The molecules are rendered as a ribbon diagram with contrasting colors for the glutaminase (bottom) and cyclase (top) domains. The figure shows the 15° difference in orientation of the domains in the two structures. Ala 393 and Gln397, shown as ball-and-stick near the domain interface, form hydrogen bonds with the glutaminase domain of yeast IGPS. These interactions cannot form in the more open conformation in crystals of bacterial IGPS (*13*). The oxyanion strand is shown in magenta.

with the main-chain amides of Gly524 (fα8′), Ala523 (fα8′), Gly475 (fβ6−α6), and Gly501 (fβ7−α7) (Figure 4). The glycerol hydroxyl groups form direct or water-bridged hydrogen bonds with the side chains of conserved residues Asp245 (fβ1), Lys258(fβ1−α1), Asp474 (fβ6−α6), and Ser500 (fβ7−α7). The AICAR end of PRFAR likewise has clear electron density. The AICAR phosphate interacts with Thr365, Gly332, and Gly364. The ribose hydroxyl groups form hydrogen bonds with the side chains of Ser402 and conserved Asp404 (fβ5).

The aminoimidazole carboxamide group at the AICAR end of PRFAR is sandwiched between the fβ2−fα2 and fβ5−fα5 loops of the enzyme (Figure 2). Conserved residues Ile299 and Gly442 on these loops move 1 Å closer together upon PRFAR binding and are in van der Waals contact with the carboxamide. The aminoimidazole ring and its carboxamide substituent are coplanar, and form no hydrogen bonds with the protein in this crystal structure. Coplanarity results in an intramolecular hydrogen bond between the carboxamide and the imidazole N substituent (N6). However, the carboxamide N and O atoms cannot be distinguished in electron density at 2.5-Å resolution, nor can their identities be established by donor/acceptor requirements due to the lack of hydrogen bonds to protein atoms. Thus, the intramolecular H-bond could be between carboxamide C═O and amine NH, or between carboxamide NH_2 and imine N, dependent on the tautomeric state of the bridging atoms N6, C7, and N8 (Figure 1). The electron density map is not definitive on this

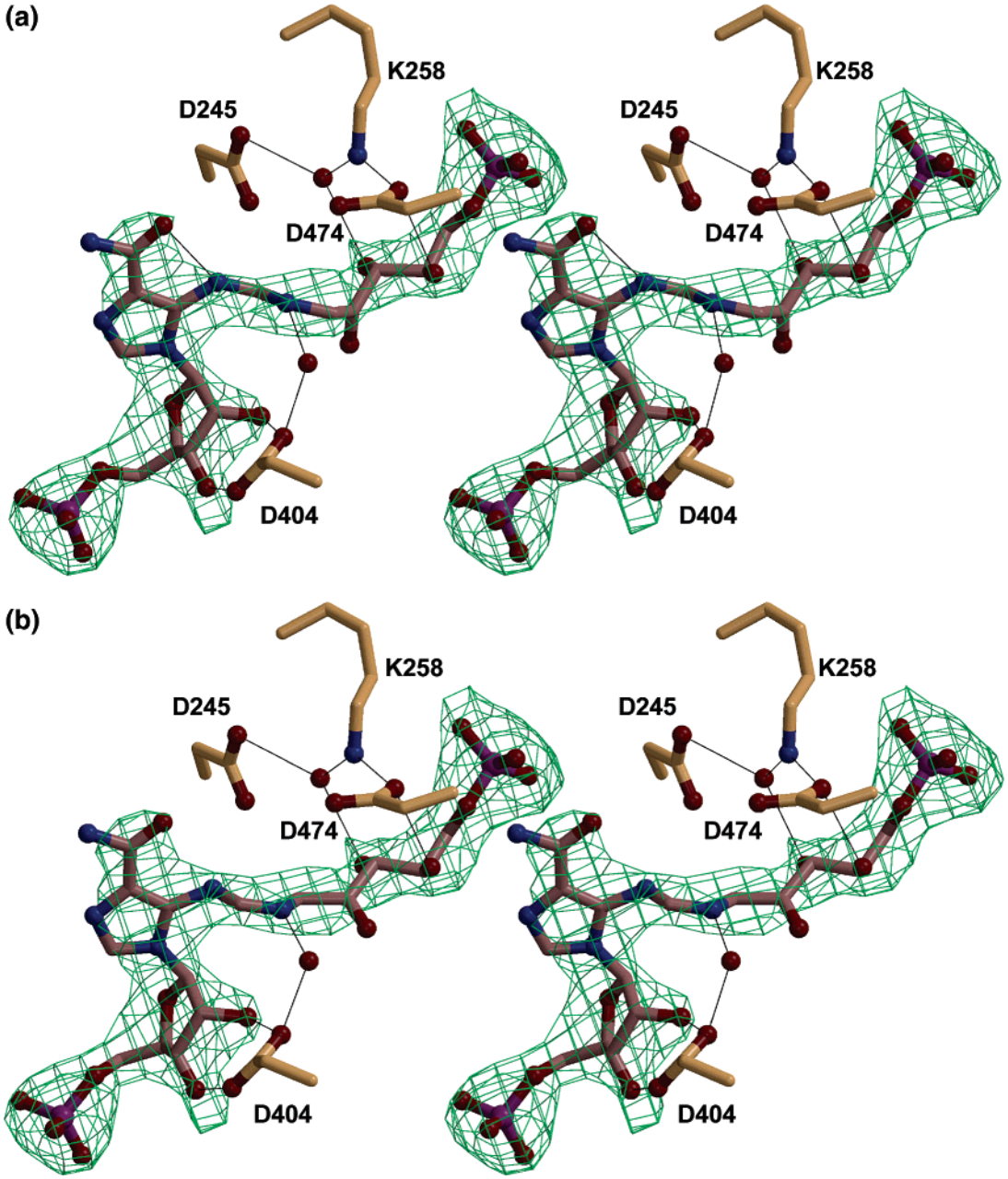

FIGURE 3: PRFAR in the cyclase active site of IGPS. Electron density from a simulated-annealing omit map is contoured in green at three times the RMS level in these stereo diagrams. Chemical groups implicated in catalysis (Asp245, Lys258, Asp404, Asp474, and waters 407 and 409) are shown with the (a) *trans*-eclipsed and (b) *cis*-extended forms of PRFAR, which fit the density equally well. The entrance to the NH_3 tunnel in the $(\beta/\alpha)_8$ barrel domain is at the lower right corner of these diagrams.

point, but we find only one chemically reasonable, density-compatible interpretation. A full PRFAR molecule with acceptable bond lengths and angles could be built into density if it had a C7−N8 double bond (coplanarity of N6−C7−N8−C1′), but not if it had an N6−C7 double bond (nonplanarity of C5−N6−C7−N8). We therefore conclude that the imidazole N substituent (N6) is an amine, not an imine, and that the intramolecular hydrogen bond is between carboxamide C═O and amine NH. This result is consistent with catalytic cleavage of the N6−C7 bond. The enzyme is expected to bind the substrate in a conformation incompatible with a double bond at N6−C7.

While electron density is continuous for PRFAR, the conformation is least clear for the central five atoms, destined to become part of the imidazole ring (Figure 3). Two chemically sensible conformers fit the density equally well: one with a *trans* double bond at C7−N8 and an eclipsed conformation at the N8−C1′ bond (Figure 3a); the other with a *cis* double bond at C7−N8 and an extended conformation at the N8−C1′ bond (Figure 3b). The central carbonyl oxygen, which lacks density and also hydrogen bonds, is in different positions in the "*trans*-eclipsed" and "*cis*-extended" conformers. Of the two conformers, the *trans*-eclipsed with its eclipsed N8−C1′ bond is more similar to the product ImGP, in which C7, N8, C1′, C2′ and glutamine-derived N form the imidazole ring. The *trans*-eclipsed conformer is also consistent with the intramolecular H-bond described above while the *cis*-extended conformer is not.

The largest change to the enzyme structure induced by PRFAR binding is a reorientation of the partially ordered fβ1−α1 loop (residues 247−275). The protein backbone

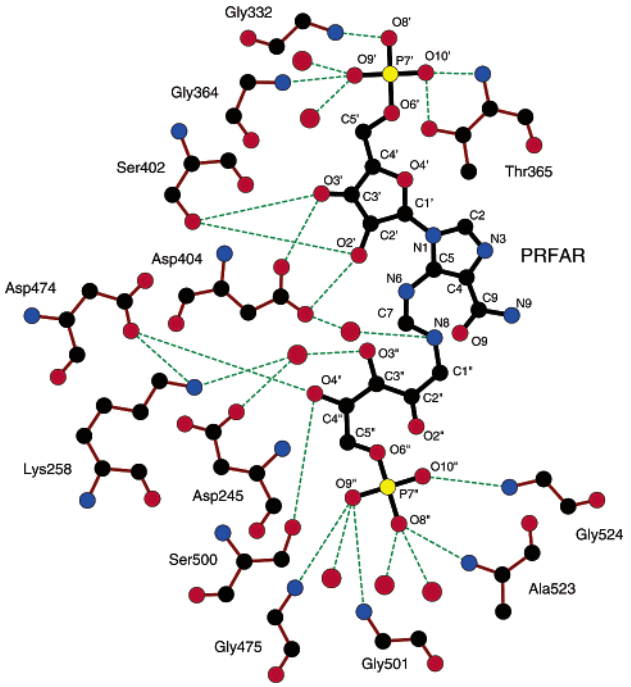

FIGURE 4: Hydrogen bonding interactions of PRFAR. Hydrogen bonds are depicted as dashed lines in the schematic diagram. Atomic nomenclature for PRFAR is indicated.

between residues 256 and 258 moves 5−10 Å toward the active site, causing the side chain of conserved Lys258 to point into the active site (Figure 2a), where it is in position to form favorable electrostatic interactions with conserved Asp474 (fβ6−α6), with the PRFAR glycerol phosphate (3.6 Å), and with conserved Asp245 (fβ1) through a water molecule (Figure 4). Remarkably, interaction of Lys258 with bound substrate in the active site does not induce ordering of the loop in this crystal structure. Lys258 is the last residue of the fβ1−α1 loop with electron density. Other active site loops at the top of the barrel "squeeze" slightly around bound PRFAR by moving in from the sides of the long, narrow active site cleft. The structural changes we observe upon PRFAR binding are limited by the crystal lattice. Prolonged soaking times and more concentrated PRFAR solutions destroy the crystals, an observation unique to PRFAR soaks. Even larger structural changes are expected in solution.

States of the Glutaminase Active Site. The active site of the glutaminase domain is comprised of the catalytic triad residues (Cys83−His193−Glu195) typical of the Triad amidotransferases (*5*). A recurring feature of Triad amidotransferases is a five-residue motif (G_{81}−X−C−X−G_{85}) known as the "nucleophile elbow", nearly identical to that first described in the unrelated α/β hydrolases (*34*). The amidotransferase nucleophile elbow is flanked on one side by a catalytic loop housing the other two components of the catalytic triad, His193 and Glu195, and on the opposite side by an "oxyanion" strand, residues 44−51. Residues of the Cys−His−Glu triad are positioned identically in all IGPS structures. By analogy to other triad amidotransferases, the oxyanion strand is thought to provide a suitably positioned amide group to stabilize the transient oxyanion of the tetrahedral intermediate during glutamine hydrolysis. However, unlike other members of the triad family, the oxyanion hole of IGPS is not formed as expected in IGPS structures (*4*, *13*, *23*, *24*). In all these structures, the peptide between Gly49 and Val50 is oriented with the C═O rather than the NH pointed into the active site. Thus, the carbonyl oxygen of Gly49 blocks the expected oxyanion hole.

In addition to the unexpected conformation of the oxyanion peptide, the structure of acivicin-inactivated Cys83 differed slightly from chemical expectations, and the extent of inactivation was incomplete (*4*). To clarify the situation in the glutaminase active site, we investigated structures of apo IGPS, and of IGPS inactivated by the glutamine analogue DON.

Apo IGPS. In the structure of the apo-enzyme, the predominant conformation of the oxyanion strand is very similar to that seen in the acivicin-inactivated enzyme (Figure 5a). However, positive electron density adjacent to Val50 and high temperature factors for the carbonyl oxygen of Gly49 are consistent with conformational variability in this region of the structure.

IGPS−DON Binary Complex. The glutamine analogue DON modified Cys83 in a manner similar to acivicin. The DON covalent adduct differs from the thioester of glutamate, the presumed reaction intermediate, by addition of a methylene function so the adduct is a stable thioether. The α-amino and α-carboxyl functions of DON were well ordered and interacted with the same glutamine specificity elements as the analogous groups of acivicin. However, DON was poorly ordered at the end bonded to Cys83, and it was not possible to fix the orientation of the carbonyl oxygen mimicking the catalytic oxyanion. This result differs from the DON complex of glutamine PRPP amidotransferase, in which the adduct was well ordered and the carbonyl oxygen formed two hydrogen bonds in the oxyanion hole (*35*). Like the other IGPS structures, the oxyanion hole of the DON-inactivated enzyme was blocked by the carbonyl oxygen of Gly49. Elsewhere, 30 Å away from the site of DON inactivation, residues 301−304 in the fβ2−α2 loop of the cyclase domain are ordered in the IGPS−DON complex, but were disordered in the other yeast IGPS structures.

The IGPS−DON and apo IGPS structures demonstrate that the unexpected conformation of the oxyanion strand in the acivicin-inactivated enzyme is not an artifact of acivicin binding. Two potentially important contacts between the cyclase and glutaminase domains were identified (Figure 2b). Gln397(fα4−β5) interacts directly with the substrate glutamine, as exemplified by both analogues, acivicin and DON. Gln397 is in an identical conformation in the bound and free forms of fungal and bacterial IGPS (*4*, *7*, *12*, *13*, *23*). Likewise, other cyclase residues that face the domain interface are in virtually identical positions in all these structures. The Gln397 side chain conformation is fixed by a hydrogen bond between the side chain carbonyl and the backbone NH. The importance of Gln397 to glutaminase activity was identified previously in a random mutagenesis screen for substitutions in HisF that affected glutaminase in HisH (*2*). The second important interdomain contact is a hydrogen between backbone atoms of Ala393 and Asn52. This contact is a direct link between the cyclase domain and the oxyanion strand.

DISCUSSION

PRFAR Active Site. IGPS binds PRFAR in a deep cleft stretching across the top of the $(\beta/\alpha)_8$ barrel of the cyclase

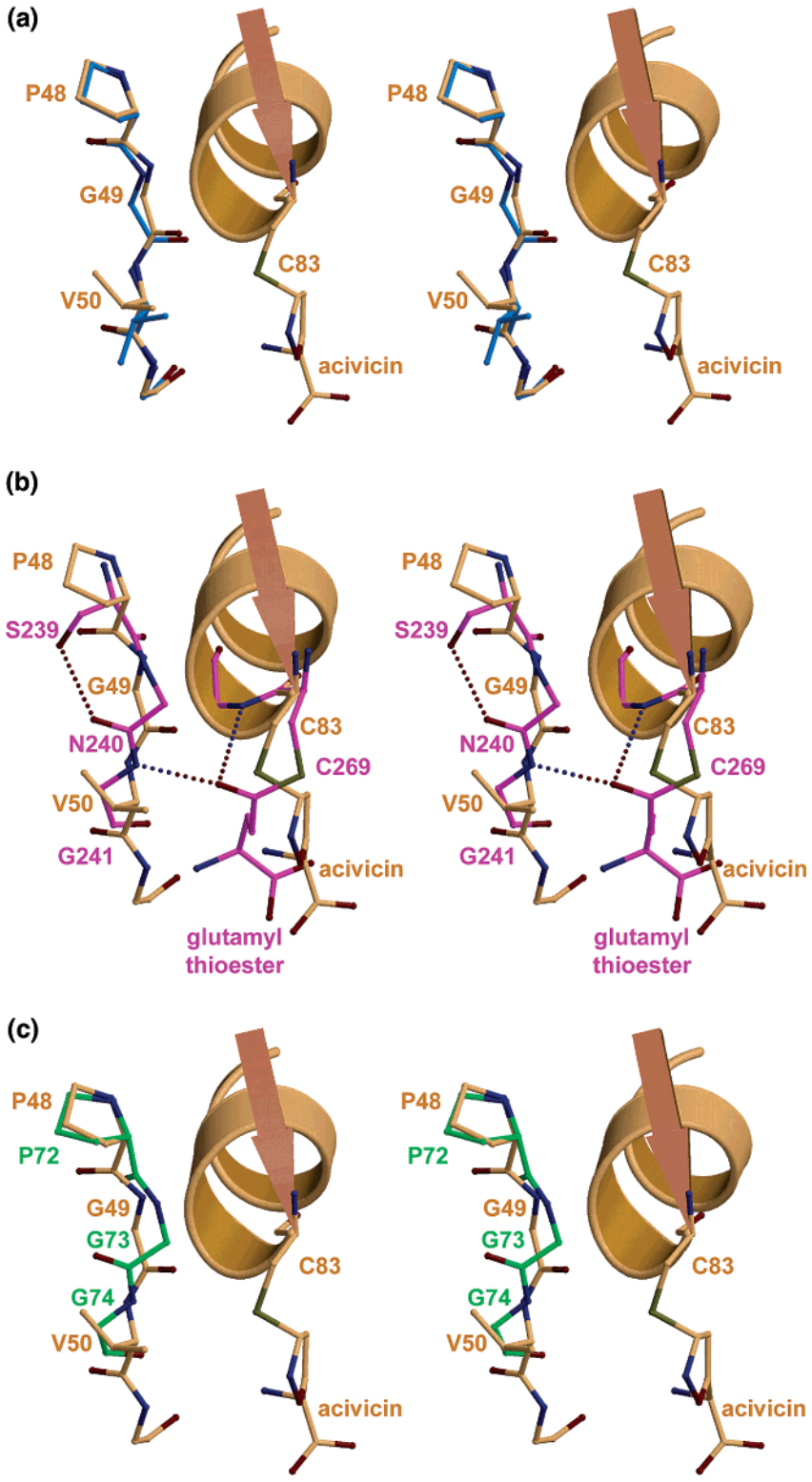

FIGURE 5: Comparison of oxyanion stabilization by proteins of the Triad amidotransferase family. In these stereo diagrams, the acivicin adduct of Cys83 in IGPS and the adjacent oxyanion strand are shown in stick form with atomic coloring (yellow C, red O, blue N, green S). Cys83 is at the junction of strand hβ3 (arrow) and helix hα2 (helical ribbon). The acivicin adduct of IGPS is superimposed with the same regions of (a) apo-IGPS (blue C), (b) the glutamate thioester of carbamoyl phosphate synthase (magenta C) (*36*), and (c) γ-glutamyl hydrolase (green C) (*40*). The thioester O forms two hydrogen bonds in the oxyanion hole of carbamoyl phosphate synthase (b), one with a backbone NH in the oxyanion strand. The orientation of this peptide is stabilized by a hydrogen between the peptide C═O and the Ser hydroxyl of the preceding residue. In IGPS, the oxyanion hole is unformed because the Gly49−Val50 peptide is oriented with its C═O blocking the presumed oxyanion hole; the preceding residue, Pro48, is incapable of hydrogen bonding. The IGPS oxyanion strand exhibits conformational variability (a), but in all cases the oxyanion hole is blocked. The properly formed oxyanion hole of γ-glutamyl hydrolase (c) illustrates that a Pro side chain at the position analogous to Pro48 of IGPS does not preclude formation of the oxyanion hole.

domain. Several loops surrounding the active site move slightly toward PRFAR. However, the conformational changes induced by substrate binding are incomplete. Additional protein conformational changes occurred upon extended

exposure of crystals to PRFAR, but were incompatible with the crystal lattice and destroyed diffraction. Therefore, we characterize the observed PRFAR complex as precatalytic.

PRFAR is in an extended conformation with the terminal phosphate groups bound to previously identified sites on the enzyme. An important feature of substrate binding is the specificity of the enzyme for the PRFAR tautomer that is optimal for cleavage of the N6−C7 bond. The PRFAR structure with a double bond between C7 and N8 and a single bond between N6 and C7 is most compatible with the electron density and also most consistent with the reaction chemistry.

However, it was not possible to distinguish between conformers of PRFAR with C7−N8 *cis*, N8−C1″ extended and with C7−N8 *trans*, N8−C1″ eclipsed, due to the diffraction limit of the crystals and/or the presence of multiple conformers. The productive Michaelis complex likely involves a single conformer of PRFAR. The *trans*-eclipsed form should be greatly preferred over the *cis*-extended for the cyclization step of the reaction and further discussion will be restricted to this model. How the enzyme differentiates between the unwanted *cis* and favorable *trans* forms is not obvious in this structure.

The mechanism of PRFAR breakdown to ImGP and AICAR involves (in unknown order) (i) a C−N bond break (C7−N6), (ii) a NH_3-dependent C−N bond formation (C2″-NH_3), (iii) a methylene hydrogen abstraction (C1″) and (iv) a cyclization step (-C7−N8−C1″−C2″−NH_3-) to form the imidazole ring of ImGP. Mutational and kinetic studies of *T. maritima* IGPS demonstrated essential roles for Asp245 and Asp404 (*11*). These residues are pseudosymmetric counterparts on the fβ1/α1 and fβ5/α5 loops of the pseudosymmetric $(\beta/\alpha)_8$ cyclase barrel. The yeast IGPS−PRFAR complex structure described here shows the strategic positions of these two residues around the active site (Figure 4). Asp404 is hydrogen bonded to both hydroxyl groups of the ribose ring and has a water-bridged (W407) interaction with N8 of PRFAR. The Asp404−W407 pair may act as a catalyst. *T. maritima* IGPS with Asp404 substituted by glutamate is active, but an asparagine substutition is inactive, indicating that the Asp404−water pair may be the catalytic base. Water 407 is also near enough to C1″ to assist in methylene-hydrogen abstraction by polarizing the methylene group via a C1″H- -:OH_2 hydrogen bond.

Asp245 forms a water-bridged hydrogen bond with a glycerol hydroxyl group of PRFAR. The analogue of Asp245 is essential for activity in *T. maritima* HisF, and was proposed to be a catalytic acid (*11*). The $O_{\delta 1}$ atom of Asp245 is 5.0 Å from C7 and 5.7 Å from C2″ of PRFAR. To be a catalyst, Asp245 would need to move closer to the substrate. Its current position may be a feature of the precatalytic complex. PRFAR appears to have a looser fit to the Asp245 side of the active site (lined by strands fβ1, fβ2, and β3) and a more hand-in-glove fit to the other side (lined by strands fβ5, fβ6, and fβ7, including Asp404 and Asp474).

The enzyme orients the reactive part of PRFAR toward the NH_3 tunnel for nucleophilic attack (Figures 2b and 3a). The C2″ carbonyl of PRFAR sits directly over the tunnel and thus might be a suitable candidate for attack by NH_3. However, the top of the tunnel is wide enough that attack at the nearby C7 cannot be ruled out, i.e., the labile C7−N6 bond may break before or coincident with NH_3 attack.

The Glutaminase Active Site. The positions of residues in the catalytic triad and in the glutamine specificity pocket are identical in the free enzyme and in the acivicin- and DON-inactivated forms of yeast IGPS. This substantiates the finding that glutamine can bind IGPS even in the absence of PRFAR but cannot be hydrolyzed at an appreciable rate (*14*). However, the structures presented here lack an oxyanion hole to stabilize the transient negative charge on the oxygen atom of the tetrahedral intermediate in glutamine hydrolysis. An oxyanion hole is expected to consist of the backbone NHs of Val84 and Val50, by analogy to structures of other triad amidotransferases in which these groups are oriented for hydrogen bonding to a single oxygen atom (Figure 5b). However, the putative oxyanion hole of IGPS is blocked by the C═O of Gly49, and the NH of Val50 points away from the active site (Figure 5a). The IGPS structures support a model in which a blocked oxyanion hole is the primary impairment to glutaminase activity in absence of a signal from the cyclase active site. Several lines of evidence support this model. All of our structures have residual positive electron density near the critical oxyanion peptide (residues 49−50), indicative of multiple conformers. However, in each case, the C═O of the Gly49−Val50 peptide points into the active site. In the acivicin-inactivated enzyme, the isoxazole ring is not oriented as expected, and no part of the analogue occupies the putative oxyanion hole (Figure 5a). In the DON-inactivated enzyme, the thioether connection to Cys83 is poorly ordered, apparently because the carbonyl group of the analogue cannot bind in the blocked oxyanion hole. This is in striking contrast to the structure of DON-inactivated glutamine PRPP amidotransferase (*35*), in which the analogue carbonyl forms two excellent hydrogen bonds in the oxyanion hole. It is also in contrast to the structure of the glutamate thioester of carbamoyl phosphate synthetase (*36*), in which the oxygen of the glutamate thioester occupies the expected oxyanion hole (Figure 5b). Formation of the oxyanion hole may be an activating step for IGPS from all biological sources because the highly conserved, glycine-rich sequence of the oxyanion strand (Pro_{48}−Gly−Xaa−Gly_{51}) appears amenable to peptide reorientation. Indeed, in the structures of bacterial HisH and the bacterial HisH−HisF heterodimer, the analogous C═O also blocks the putative oxyanion hole (*13*, *23*, *24*). Similar proposals have been made for cysteine proteases (*37*).

In Search of the Signaling Elements. An important result of this study is the orientation of PRFAR in the cyclase active site and the implications of this finding for signaling between the cyclase and glutaminase active sites. Of the two reaction products, ImGP stimulates glutaminase activity in the remote active site to a greater extent than does AICAR (*14*). Thus, interactions and conformational changes at the glycerol phosphate end of PRFAR merit special attention. These interactions involve residues in strand fβ1, in helix fα8′, and in loops fβ6−α6, fβ7−α7, fβ8−α8, and fβ1−α1. Asp474 (fβ6−α6) and Lys258 (fβ1−α1) form a salt link (Figure 4), which does not exist in structures lacking PRFAR. Lys258 is implicated in signaling because a serine substitution (K19S in *T. maritima* HisF) reduces the rate of glutamine-dependent catalysis 270-fold but does not affect the NH_3-dependent reaction (*11*). How might changes in these loops be transmitted to the glutaminase active site, which is docked at the

bottom of the $(\beta/\alpha)_8$ barrel? No direct conformational changes to structures at the bottom of the barrel are apparent in the PRFAR complex of IGPS.

Comparison of the structures of yeast IGPS and the bacterial intact enzyme are suggestive of a model for signaling and activation. The heterodimeric HisF−HisH bacterial enzyme from *Thermotoga maritima* (*13*) has a more open interface between catalytic modules than does the yeast enzyme (Figure 2b). The structural difference is a hinge of 15° between catalytic modules; the *Thermus thermophilus* intact enzyme has an intermediate hinge position (*23*). Opening of the interdomain hinge eliminates direct contact between the cyclase domain and the oxyanion strand. In the yeast enzyme, the oxyanion strand in the glutaminase domain is linked to the cyclase domain by a hydrogen bond from the backbone NH of Asn52 to the backbone C═O of Ala393 (Figure 2b). The analogous atoms in the more open bacterial structure are more than 8 Å apart. A second contact of the cyclase domain to the glutaminase active site is the hydrogen bond between invariant Gln397 and the glutamine substrate analogue (Figure 2b). This contact is also impossible in the hinge-open structures. We hypothesize that completion of the conformational signal induced by PRFAR binding further closes the catalytic modules, reorganizes the oxyanion strand, and forms the oxyanion hole by flipping the peptide between residues 49 and 50. Furthermore, the hinge, which includes the fusion peptide between glutaminase and cyclase domains, is on the same side of the cyclase barrel as the glycerol phosphate moiety, the stronger "signaling" end of PRFAR.

Every glutamine amidotransferase must incapacitate its glutaminase domain until an activation signal is received from the remote catalytic domain. It appears that the amidotransferases employ a variety of mechanisms to accomplish this regulation. Among the triad amidotransferases of known structure, IGPS is unique in having a blocked oxyanion hole. The relevant NH groups in GMP synthetase (*6*), carbamoyl phosphate synthetase (*36*), and anthranilate synthase (*38*, *39*) are pointed directly into the active site. The same is true of the nonamidotransferase homologue γ-glutamyl hydrolase (*40*) (Figure 5c). The kinetic constants of basal glutaminase compared to PRFAR-stimulated glutaminase (a significantly reduced k_{cat} and an unaffected K_m) (*40*) are consistent with a blocked oxyanion hole in absence of PRFAR.

All of the structural (*4*, *13*, *23*) and biochemical (*2*, *11*, *14*) data support a signaling mechanism in which PRFAR binding induces movement of an interdomain hinge that is linked to the glycerol phosphate end of PRFAR. The structures revealed no clues of how PRFAR binding is communicated to the hinge region. Hinge movement alters key signaling contacts at the domain interface. Two such contacts have been identified between Gln397 and the glutamine substrate and between Ala393 and the oxyanion strand. The most important result of hinge movement is predicted to be unblocking of the glutaminase oxyanion hole via a "push" on the oxyanion strand from the cyclase domain. According to this model, the peptide between Gly49 and Val50 flips to remove the C═O from the active site and to move the NH into a position where it can stabilize the catalytic oxyanion. It remains to visualize this more active form of the glutaminase active site.

ACKNOWLEDGMENT

The authors thank Jianghai Zhu for helpful discussions.

REFERENCES

1. Klem, T. J., and Davisson, V. J. (1993) *Biochemistry 32*, 5177−86.
2. Klem, T. J., Chen, Y., and Davisson, V. J. (2001) *J. Bacteriol. 183*, 989−96.
3. Alifano, P., Fani, R., Lio, P., Lazcano, A., Bazzicalupo, M., Carlomagno, M. S., and Bruni, C. B. (1996) *Microbiol. Rev. 60*, 44−69.
4. Chaudhuri, B. N., Lange, S. C., Myers, R. S., Chittur, S. V., Davisson, V. J., and Smith, J. L. (2001) *Structure (London) 9*, 987−97.
5. Zalkin, H., and Smith, J. L. (1998) *Adv. Enzymol Relat. Areas Mol. Biol. 72*, 87−144.
6. Tesmer, J. J. G., Klem, T. J., Deras, M. L., Davisson, V. J., and Smith, J. L. (1996) *Nat. Struct. Biol. 3*, 74−86.
7. Lang, D., Thoma, R., Henn-Sax, M., Sterner, R., and Wilmanns, M. (2000) *Science 289*, 1546−50.
8. Fani, R., Tamburini, E., Mori, E., Lazcano, A., Lio, P., Barberio, C., Casalone, E., Cavalieri, D., Perito, B., and Polsinelli, M. (1997) *Gene 197*, 9−17.
9. Chittur, S. V., Chen, Y., and Davisson, V. J. (2000) *Protein Expression Purif. 18*, 366−77.
10. Chittur, S. V., Klem, T. J., Shafer, C. M., and Davisson, V. J. (2001) *Biochemistry 40*, 876−87.
11. Beismann-Driemeyer, S., and Sterner, R. (2001) *J. Biol. Chem. 276*, 20387−96.
12. Banfield, M. J., Lott, J. S., Arcus, V. L., McCarthy, A. A., and Baker, E. N. (2001) *Acta Crystallogr. D. Biol. Crystallogr. 57*, 1518−25.
13. Douangamath, A., Walker, M., Beismann-Driemeyer, S., Vega-Fernandez, M. C., Sterner, R., and Wilmanns, M. (2002) *Structure (London) 10*, 185−93.
14. Myers, R. S., Jensen, J. R., Deras, I., Smith, J. L., and Davisson, V. J. (2003) *Biochemisry*, 42, 7013−7022.
15. Huang, X., Holden, H. M., and Raushel, F. M. (2001) *Annu. Rev. Biochem. 70*, 149−80.
16. Krahn, J. M., Kim, J. H., Burns, M. R., Parry, R. J., Zalkin, H., and Smith, J. L. (1997) *Biochemistry 36*, 11061−8.
17. Bera, A. K., Chen, S., Smith, J. L., and Zalkin, H. (2000) *J. Bacteriol. 182*, 3734−3739.
18. Chen, S., Burgner, J. W., Krahn, J. M., Smith, J. L., and Zalkin, H. (1999) *Biochemistry 38*, 11659−11669.
19. Mullins, L., and Raushel, F. M. (1999) *J. Am. Chem. Soc. 121*, 3803−3804.
20. Huang, X., and Raushel, F. M. (2000) *J. Biol. Chem. 275*, 26233−40.
21. Thoden, J. B., Huang, X., Raushel, F. M., and Holden, H. M. (2002) *J. Biol. Chem. 277*, 39722−7.
22. Thoden, J. B., Holden, H. M., Wesenberg, G., Raushel, F. M., and Rayment, I. (1997) *Biochemistry 36*, 6305−6316.
23. Omi, R., Mizuguchi, H., Goto, M., Miyahara, I., Hayashi, H., Kagamiyama, H., and Hirotsu, K. (2002) *J. Biochem. (Tokyo) 132*, 759−65.
24. Korolev, S., Skarina, T., Evdokimova, E., Beasley, S., Edwards, A., Joachimiak, A., and Savchenko, A. (2002) *Proteins 49*, 420−2.
25. Otwinowski, Z., and Minor, W. (1997) in *Macromolecular Crystallography Part A* (Carter, J., C. W., and Sweet, R. M., Eds.) pp 307−325, Academic Press, New York.
26. Brünger, A. T., Krukowski, A., and Erickson, J. W. (1990) *Acta Crystallogr. A46*, 585−593.
27. Brünger, A. T., Adams, P. D., Clore, G. M., DeLano, W. L., Gros, P., Grosse-Kunstleve, R. W., Jiang, J. S., Kuszewski, J., Nilges, M., Pannu, N. S., Read, R. J., Rice, L. M., Simonson, T., and Warren, G. L. (1998) *Acta Crystallogr. D54*, 905−921.
28. Jones, T. A., Zou, J. Y., Cowan, S. W., and Kjeldgaard. (1991) *Acta Crystallogr. A 47 (Pt 2)*, 110−9.
29. Allen, F. H., and Kennard, O. (1993) *Chem. Des. Autom. News 8*, 31−37.
30. Bernstein, F. C., Koetzle, T. F., Williams, G. J., Meyer, E. F., Jr., Brice, M. D., Rodgers, J. R., Kennard, O., Shimanouchi, T., and Tasumi, M. (1977) *J. Mol. Biol. 112*, 535−42.

31. Kleywegt, G. J., and Jones, T. A. (1998) *Acta Crystallogr. D54*, 1119−1131.
32. Vriend, G., and Sander, C. (1993) *J. Appl. Crystallogr. 26*, 47−60.
33. Laskowski, R. A., MacArthur, M. W., Moss, D. S., and Thornton, J. M. (1993) *J. Appl. Crystallogr. 26*, 283−291.
34. Ollis, D. L., Cheah, E., Cygler, M., Dijkstra, B., Frolow, F., Franken, S. M., Harel, M., Remington, S. J., Silman, I., Schrag, J., et al. (1992) *Protein Eng. 5*, 197−211.
35. Kim, J. H., Krahn, J. M., Tomchick, D. R., Smith, J. L., and Zalkin, H. (1996) *J. Biol. Chem. 271*, 15549−15557.
36. Thoden, J. B., Miran, S. G., Phillips, J. C., Howard, A. J., Raushel, F. M., and Holden, H. M. (1998) *Biochemistry 37*, 8825−31.
37. Menard, R., and Storer, A. C. (1992) *Biol. Chem. Hoppe Seyler 373*, 393−400.
38. Knochel, T., Ivens, A., Hester, G., Gonzalez, A., Bauerle, R., Wilmanns, M., Kirschner, K., and Jansonius, J. N. (1999) *Proc. Natl. Acad. Sci. U.S.A. 96*, 9479−84.
39. Spraggon, G., Kim, C., Nguyen-Huu, X., Yee, M. C., Yanofsky, C., and Mills, S. E. (2001) *Proc. Natl. Acad. Sci. U.S.A. 98*, 6021−6.
40. Li, H., Ryan, T. J., Chave, K. J., and Van Roey, P. (2002) *J. Biol. Chem. 277*, 24522−9.
41. Kleywegt, G. J., Zou, J. Y., Kjeldgaard, M., and Jones, T. A. (2001) in *International Tables for Crystallography*, *Vol. F Crystallography of Biological Macromolecules* (Rossmann, M. G., and Arnold, E., Eds.) pp 353−356, 366−367, Dordecht: Kluwer Academic Publishers, The Netherlands.

BI034320H